Optik - International Journal for Light and Electron Optics 319 (2024) 172113

Contents lists available at ScienceDirect

Optik

journal homepage: www.elsevier.com/locate/ijleo

Original research article

Ultra-broadband mid-infrared supercontinuum generation in square lattice As_2S_3 chalcogenide photonic crystal fibers

Ben Chu Van [a], Trong Dang Van [b], Lan Phan Thi [c], Lanh Chu Van [b,*]

[a] Faculty of Electronic Engineering I, Posts and Telecommunications Institute of Technology, Hanoi, Viet Nam
[b] Department of Physics, Vinh University, 182 Le Duan, Vinh, Viet Nam
[c] Vietnam-Korea Institute of Science and Technology, Hoa Lac High-Tech Park, Hanoi, Viet Nam

ARTICLE INFO

Keywords:
Photonic crystal fiber (PCF)
Square lattice
Supercontinuum generation
All-normal dispersion
Anomalous dispersion

ABSTRACT

This work presents a numerical model of a photonic crystal fiber made up of chalcogenide glass for highly coherent supercontinuum generation in the mid-infrared spectral region. Numerical simulations based on the finite element method have been performed. An optical dispersion engineering technique has been adopted to minimize the dispersion effect at pump wavelength by alteration of geometrical parameters of designed fiber. We have selected two optimal structures from the simulation results to analyze the nonlinear characteristics and supercontinuum generation. The first fiber, $\#F_1$ with a lattice constant of 1.0 μm and a filling factor of 0.3 operates in all-normal dispersion, providing the spectrum SC in the range of 2.4 μm to 8.0 μm with a pump wavelength of 5.0 μm, pulse duration of 90 fs, and peak power of 6 kW. Meanwhile, fiber $\#F_2$ has anomalous dispersion regimes. With a peak power of 2 kW, this fiber produces a wide SCG with spectral ranges of 4.4–16 μm. The proposed structures are promising for applications in low-peak power all-fiber optical systems.

1. Introduction

Supercontinuum (SC) generation in nonlinear media originates from the interaction of ultrashort pulses and the dispersion and nonlinear effects, such as self-phase modulation (SPM), four-wave mixing (FWM), stimulated Raman scattering (SRS), soliton self-frequency shift, etc. [1–3]. It is a process in which narrowband pump pulses with high peak power are broadened continuously in the spectral domain. SC sources have been studied extensively in various nonlinear media (including solids, liquids, and gases) since 1970 when it was first reported by Alfano et al. in BK7 glass pumped by a mode-locked Nd: glass laser [4].

SC sources with spatial coherence, broad bandwidth, and high brightness have received considerable attention due to their significant potential in various applications, such as sensing [5–7], biomedical science [8], spectral tissue imaging [9,10], and optical coherence tomography [11,12]. Over the past two decades, many researchers have been devoted to extending the SC spectral range from visible and near-infrared (NIR) to ultraviolet and mid-infrared (MIR) and even far-infrared (FIR). In particular, the MIR spectral region is regarded as an important topic because most molecules exhibit fundamental vibrational absorption bands in this region [5,9,13], leaving distinctive spectral fingerprints critical for applications, such as biomedical science, sensing, and defense and security. However, SC sources generated in silica fibers are limited in the spectral evolution into MIR due to the absorption loss in silica increasing exponentially for wavelengths greater than 2.5 μm, thus SCG centered about 2.5 μm and beyond is not possible.

* Corresponding author.
E-mail address: chuvanlanh@vinhuni.edu.vn (L. Chu Van).

https://doi.org/10.1016/j.ijleo.2024.172113
Received 31 July 2024; Received in revised form 6 November 2024; Accepted 7 November 2024
Available online 8 November 2024

A promising alternative using hollow-core fibers filled with liquids with a high nonlinear refractive index and high transparency for efficient SC generation has been investigated. Infiltration of high nonlinear refractive index liquids into the core improves photonic crystal fiber (PCF)'s nonlinear coefficient, which is beneficial for SCG efficiency. According to this method, nonlinear liquids were used to obtain a broad and coherent SC spectrum [14–27]. However, the use of liquid core fibers requires complex additional systems to contain and introduce liquid completely into the core during SCG measurement [18,28,29]. Therefore, the development of an SCG system that is entirely equal to the use of liquid-core fiber is still limited.

Another attractive approach for SCG is to use optical fibers made from soft glasses, such as flouride [30–34], telluride [35,36], and chalcogenide [37–41]. Among the soft glasses, Chalcogenide (ChG) glasses are compounds that contain at least one of the chalcogen elements (S, Se, Te) combined with the other elements such as Sb, Ge, As, Ga, etc. [36,37]. ChG glasses are of great interest due to the possibility of producing glass systems with large composition space and good resistance to crystallization which yield excellent optical properties such as high refractive indices, high Kerr nonlinearities, and broad transparency window extending from near-infrared to mid-infrared wavelengths [38,39]. Owing to these excellent optical properties, ChG glasses have been extensively employed in designing mid-infrared SC laser sources.

These beneficial features of ChG glass, combined with the high flexibility of PCF design, have been recently exploited with several numerical and experimental demonstrations of efficient mid-infrared and coherent SC sources, realized by pumping femtosecond laser pulses [40–47]. Shaw et al. experimentally demonstrated the broadening of the SC spectrum from 2.1 to 3.1 μm using a PCF in As_2Se_3 chalcogenide glass [40]. Lanh et al. [41] achieved multi-octave SCG using As_2Se_3 chalcogenide PCF for input pulse at the wavelength of 3.5 μm. Mid-IR SC spectra, spanning 1.4–13.3 μm are reported by Petersen et al. using a chalcogenide step-index fiber [42]. A composite PCF of As_2Se_3 glass and tellurite is modeled by Liao et al. to get high nonlinearity at 1.55 μm [43]. An equiangular spiral-shaped PCF structure is theoretically presented by Saini et al. to generate the SC spectrum, spanning 1.2–15 μm [44]. Salem et al. conducted numerical investigations of a tapered As_2S_3 PCF design using a pulse energy of 100 pJ pumping at 4.7 μm for the generation of an ultra-broadband SC spectrum [45]. Numerical modeling of an As_2Se_3 rib waveguide is also reported by Saini et al. for SCG [46]. Using a Ge-Sb-S chalcogenide-based waveguide, nonlinear characterization is carried out by Choi et al. for the demonstration of the SC spectrum [47].

Almost all of the aforementioned analytical works employ the chalcogenide PCF with small core diameter for mid-IR SCG. The fact that the PCF has a small core with high confinement loss reduces the spectral broadening and brightness of the SCG at long wavelengths. Moreover, the small core fiber offers a low coupling efficiency of the light from the laser into the fiber core in SCG measurement. Besides, the dispersion of previous works is still limited in terms of flatness in the long wavelength range, resulting in limited SCG performance.

To overcome those limitations, we have proposed a novel aquare lattice As_2S_3 chalcogenide photonic crystal fiber structure for an ultra-broadband supercontinuum generation in the mid-IR region. Optical properties of PCFs with various lattice constant Λ and filling factor d/Λ are numerically investigated in the mid-IR range. Chromatic dispersion and linear properties have been thoroughly analyzed by taking into account the effects of the lattice constant Λ and the filling factor d/Λ. The designed chalcogenide PCF exhibits a flat dispersion profile and high nonlinearity with a low effective mode area. Supercontinuum generation performed with optimized fibers demonstrates a greater bandwidth than previous works, achieved with low peak power.

The rest of this paper is organized as follows: In Section 2, we present the proposed microstructured PCF. Section 3 shows the optimization of the characteristic quantities. The extended SC spectrum is generated in optimized PCFs with lower peak power compared with the previous works described in Section 4. The paper concludes with Section 5.

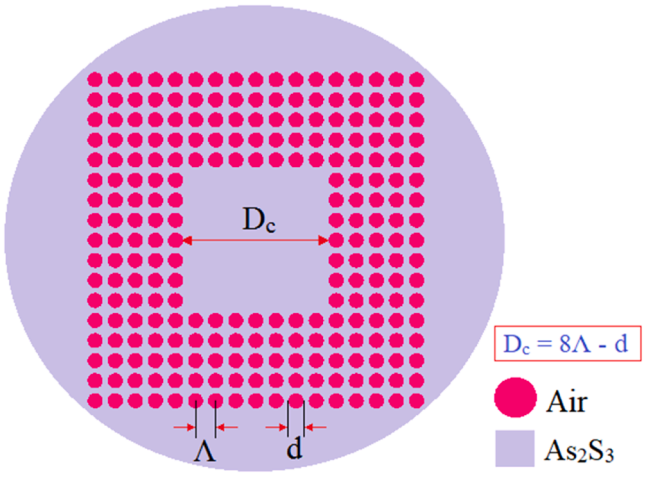

Fig. 1. Geometrical structures of large solid core PCFs with square lattice and As_2S_3 substrate.

2. Numerical modeling

Ansys Lumerical Mode software [48] was utilized to design new PCF structures with As_2S_3 substrates. The proposed PCF design can be fabricated by drilling method [49]. In Fig. 1, a cross-sectional view of the proposed design is shown. The PCF structures consist of seven air-hole rings arranged in a square lattice. As_2S_3 is a substrate material with a high nonlinear refractive index to produce the difference between core and cladding, $n_2 = 4.20 \times 10^{-18}$ m^2/W [50]. The core diameter is determined by the formula $D_c = 8\Lambda - d$, where Λ and d are lattice constant and the diameter of the air holes, respectively. The PCF nonlinearity is controlled by d/Λ and is obtained by the finite element method. The filling factor d/Λ varies from 0.3 to 0.5. The selected lattice constants for the survey include $\Lambda = 1.0$ μm, $\Lambda = 1.5$ μm, $\Lambda = 2.0$ μm, and $\Lambda = 2.5$ μm. A perfect matching layer (PML) was added to keep the accuracy of the simulation results.

The dispersive properties of optical glasses are often modeled through the Sellmeier formula. Therefore, the frequency dependence of the As_2S_3 ChG glass refractive index is given by:

$$n^2(\lambda) = 1 + \frac{8.983\lambda^2}{\lambda^2 - 0.0225\mu m^2} + \frac{1.9222\lambda^2}{\lambda^2 - 0.0625\mu m^2} + \frac{0.8765\lambda^2}{\lambda^2 - 0.1225\mu m^2} \tag{1}$$

Where λ denotes the pump wavelength in micrometers. Fig. 2 shows the evolution against wavelengths of the As_2S_3 ChG glass refractive index.

3. Optimization of the characteristic quantities of PCF

We only present the fundamental mode dispersion. The chromatic dispersion (D) of a PCF includes both the material dispersion and the waveguide dispersion, which can be defined using the following equation [1]

$$D = -\frac{\lambda}{c}\frac{\partial^2 \mathrm{Re}[n_{\mathrm{eff}}]}{\partial \lambda^2}. \tag{2}$$

where n_{eff} is the effective refractive index of a guided mode calculated using the FDE method, λ is the wavelength, and c is the velocity of light in a vacuum. Re[n_{eff}] is the real part of n_{eff}. The effective refractive index of the mode is given by $n_{eff} = \beta[\lambda, n_m(\lambda)]/k_0$, β is the propagation constant, $k_0 = 2\pi/\lambda$ is the free-space wave number, and $n_m = n_m(\lambda)$can be computed by the Sellmeier equations (Eq. 1).

Nonlinearity in the PCF is an important parameter for SC generation. In order to get accurate results, the nonlinear coefficient γ needs to be studied. The nonlinear parameter is defined as [1]:

$$\gamma = \frac{\omega_0}{c}\left(\frac{n_2}{A_{eff}}\right) = \frac{2\pi}{\lambda}\left(\frac{n_2}{A_{eff}}\right). \tag{3}$$

where,$\omega_0$is the frequency in free space, and n_2 is the nonlinear index coefficient and has units of m^2/W (As_2S_3 is estimated at 4.20×10^{-18} m^2/W [50]). As a result,γhas units of W^{-1}/m. The effective mode area A_{eff} is the wavelength-dependent effective area of propagating fundamental mode in the PCF. A_{eff} is calculated using equation [1]:

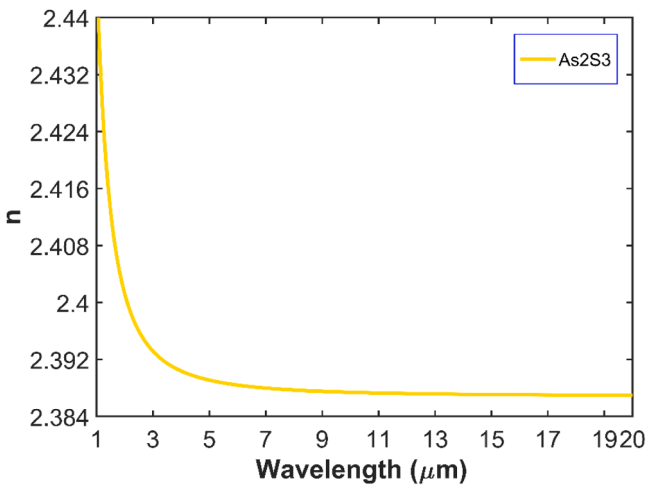

Fig. 2. Real parts of the refractive index of As_2S_3.

$$A_{\text{eff}} = \frac{\left(\int_{-\infty}^{\infty}\int_{-\infty}^{\infty}|E(x,y)|^2 dxdy\right)^2}{\int_{-\infty}^{\infty}\int_{-\infty}^{\infty}|E(x,y)|^4 dxdy} \tag{4}$$

where E (x,y) is the electric field transverse distribution of the fundamental mode. A_{eff} depends on fiber parameters such as the core radius and the core-cladding index difference. A_{eff} has units of μm^2.

Fig. 3 shows the dependence of dispersion characteristics on wavelength and the variation f of the PCF. These graphs show that the dispersion characteristics depend significantly on the diameter of the air holes and the lattice constant. PCF has a small-core diameter (Λ =1.0 μm), and dispersion characteristics are quite diverse with all-normal or anomalous dispersions with one and two zero-dispersion wavelengths (ZDW), and relatively large slopes (Fig. 3a). This is because with a smaller core, the dispersion of the waveguide is more obvious, and therefore the total dispersion curve changes more strongly. In the investigated wavelength region, all-normal dispersion is found when $f = 0.3$. In particular, we observe that the dispersion is flat and closest to the horizontal axis in the case of $f = 0.3$. The normal flat dispersion is very beneficial for the efficiency of SC generation in extending the output pulse.

Meanwhile, in PCFs with larger cores ($\Lambda = 1.5$ μm, $\Lambda = 2.0$ μm, $\Lambda = 2.5$ μm) (Fig. 3b-d), the all-normal dispersion characteristics disappear in the investigated wavelength region, leaving only anomalous dispersions with one or two ZDWs. Furthermore, for a given value of Λ ($\Lambda > 1.0$ μm), ZDW shifts towards longer wavelengths as the filling factor f is reduced. While, for some values of filling factor f, ZDW shifts towards shorter wavelengths as the Λ is reduced.

Since dispersion is one of the significant factors for the SCG, the fiber with flat dispersion allows for obtaining further broad SCG. Thus, the goal of optimization of dispersion herein is to show the fiber structures with flat near-zero dispersion shape, and the ZDW compatible with the pump wavelength. Relying on the preliminary simulation, three fibers with structure parameters as shown in Table 1 are selected to analyze the SCG because they have the flat near-zero dispersion in the mid-IR range. They are labeled as #F_1 ($\Lambda = 1.0$ μm, $d/\Lambda = 0.3$), #F_2 ($\Lambda = 2.5$ μm, $d/\Lambda = 0.3$). The fibers with $\Lambda = 1.0$ μm can offer flat all-normal dispersion, however, they have a smaller core diameter than that of #F_2 fiber. The small core results in a high confinement loss at the long-wavelength range, and thus,

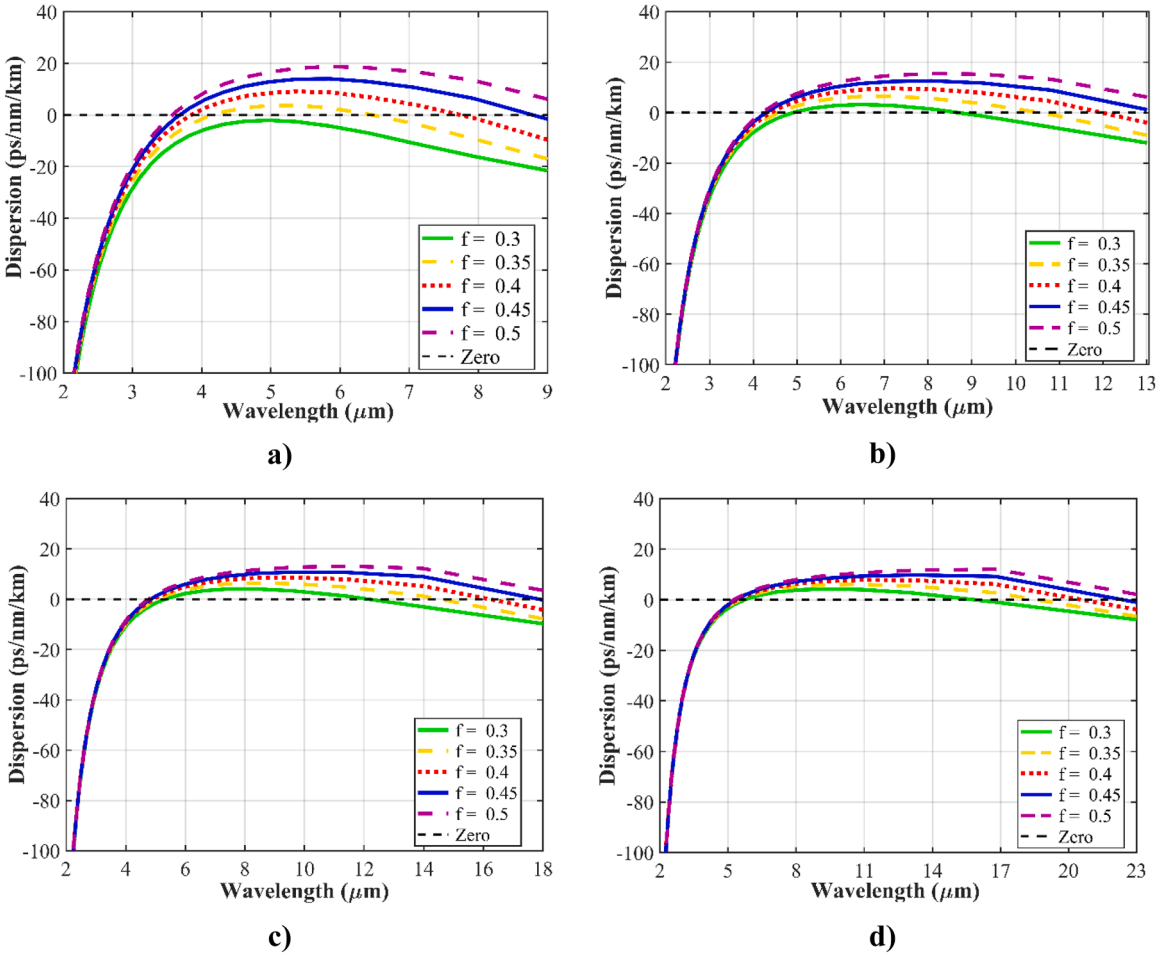

Fig. 3. Characteristics of chromatic dispersion of the fundamental mode for PCFs with hexagonal lattice with **(a)** $\Lambda = 1.0$ μm, **(b)** $\Lambda = 1.5$ μm, **(c)** $\Lambda = 2.0$ μm, and **(d)** $\Lambda = 2.5$ μm.

Table 1
The structure parameters of proposed PCFs.

Parameter	$\#F_1$	$\#F_2$
Lattice constant [μm]	1.0	2.5
Filling factor d/Λ	0.3	0.3
Core diameter D_c [μm]	7.7	19.7

it reduces the spectral broadening and brightness of SCG in the long-wavelength range. $\#F_1$ fiber has a flat all-normal dispersion. The dispersion varies from −40 to −2.0 ps/nm/km in the wavelength range of 4–7 μm, and it is further flat in the longer wavelength range. At λ = 5.0 μm, the dispersion is −2.3 ps/nm/km, Fig. 4. Thus, $\#F_1$ fiber is used for broad all-normal dispersion SCG. Meanwhile, $\#F_2$ fiber has two ZDWs at 5.5 μm (ZDW_1) and 16.2 μm (ZDW_2). The maximum value of anomalous dispersion is 4.28 ps/nm/km at 9.24 μm, Fig. 4. $\#F_2$ fiber is used for broad soliton-induced SCG. The dispersion of the $\#F_2$ at the pump wavelength is 4.18 ps/nm/km. The confinement loss characteristics (L_c) of the fundamental mode for $\#F_1$ and $\#F_2$ fibers are determined in Fig. 4(b). In the wavelength region from 1.5 μm to 4.5 μm, there is not much difference in the value of both fibers. The confinement loss of $\#F_1$ fiber increases suddenly when the wavelength is greater than 4.5 μm, while $\#F_2$ fiber has a lower confinement loss. In particular, the confinement loss of $\#F_2$ fiber is the lowest, this curve almost coincides with the horizontal axis in the range wavelength of 1.5 μm-6.0 μm, from the wavelength of 6.0 μm onwards L_c gradually increases to a value greater than 1700 dB/m.

The effect of the wavelength change (λ) on the effective mode area (A_{eff}) of the proposed PCFs is shown in Fig. 5(a). The results from the figure show that the effective mode area of both fibers increases linearly with increasing wavelength. Because of the large core diameter, the effective mode area of $\#F_2$ is always larger than the other case. At the pump wavelength, the fibers #F1, $\#F_2$ have effective mode area values of 43.8 μm^2 and 226.3 μm^2, respectively. The nonlinear coefficient is inversely proportional to the effective mode area according to Eq. 6, so it tends to decrease linearly with an increase of wavelength, Fig. 5(b). The nonlinearity of the fiber $\#F_1$ is always greater than $\#F_2$, and at the pump wavelength, the former has a nonlinear value of 120.4 $W^{-1}.km^{-1}$ while that of $\#F_2$ is 12.3 $W^{-1}.km^{-1}$.

4. Supercontinuum generation in optimized PCFs

We performed a numerical simulation of SC generation for two proposed fibers $\#F_1$ and $\#F_2$. In the simulations. The laser pulses used in the simulation were modeled by Gaussian pulses centered at the pump wavelength with P_0 as peak power, t_0 as pulse duration, and displayed in Eq. 5 [1].

$$A(T) = \sqrt{P_0}\exp\left(\frac{-T^2}{2t_0^2}\right) \tag{5}$$

The nonlinear propagation process of the pump pulse in the PCF can be described by the Schrödinger equation (GNLSE) using the symmetry split-step Fourier transform method [1], which is given by the formula:

$$\partial_z\widetilde{A} - i\widetilde{\beta}(\omega)\widetilde{A} - \frac{\widetilde{\alpha}(\omega)}{2}\widetilde{A} = i\gamma\left(1+\frac{\omega-\omega_0}{\omega_0}\right)\widetilde{A}F\left[\int_{-\infty}^{\infty} R(T')|A|^2(T-T')dT'\right]. \tag{6}$$

where α is the loss coefficient andβ is the dispersion in the frequency domain of the optical fiber.

The response function, including the Raman and Kerr nonlinearities, is represented by:

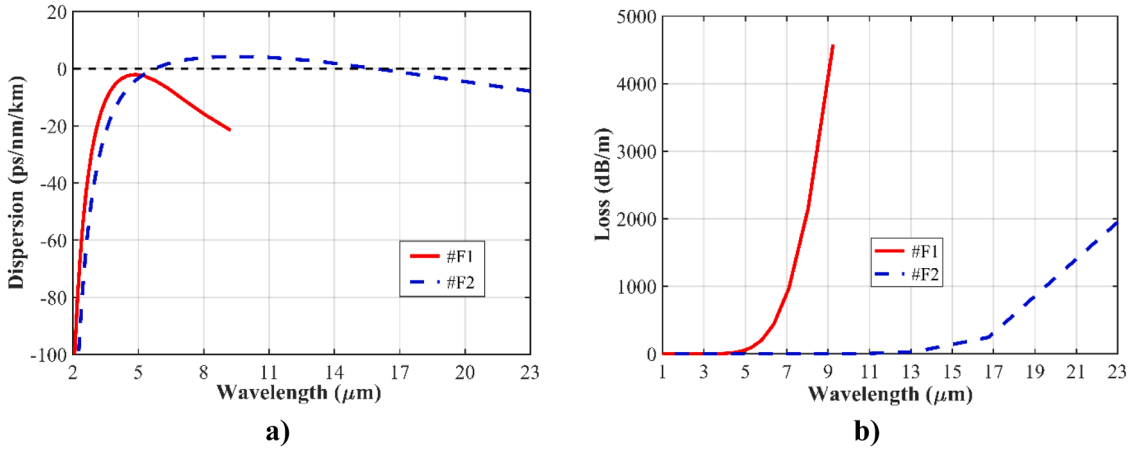

Fig. 4. a) The dispersion characteristics and b) The confinement loss of the fundamental mode for $\#F_1$ and $\#F_2$ fiber.

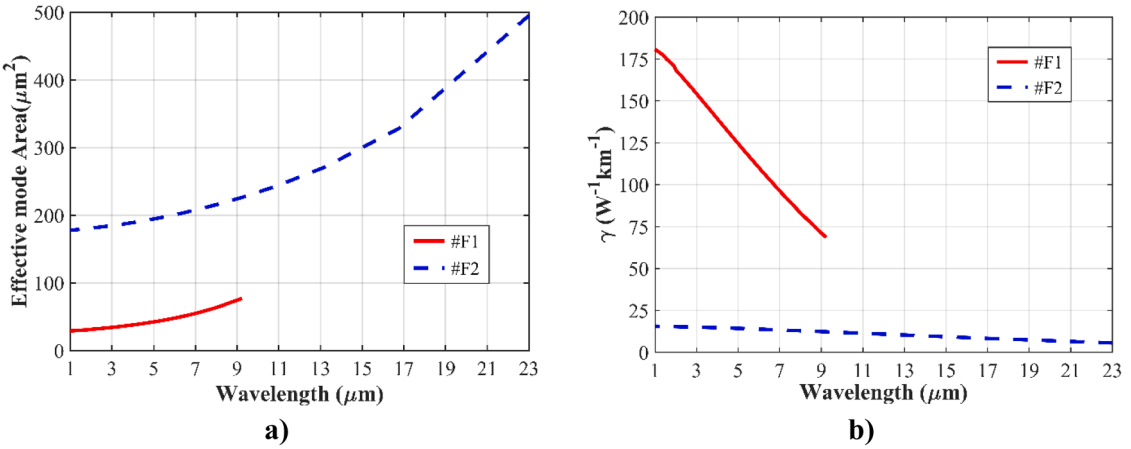

Fig. 5. a) The effective mode area and b) the nonlinear coefficient of the fundamental mode for #F_1 and #F_2 fiber.

$$R(t') = (1 - f_R)\delta(t' - t_e) + f_R h_R(t') \tag{7}$$

where (τ_1) and (τ_2) are Raman duration and lifetime, f_R and $h_R(t')$ are respectively fractional contributions of the Raman response and Raman response function [32]

The Raman response function, h_R is generally given by the following relation [1]:

$$h_R\left(t'\right) = \frac{\tau_1^2 + \tau_2^2}{\tau_1} \exp\left(\frac{-t'}{\tau_2}\right) \sin\left(-\frac{t'}{\tau_1}\right) \tag{8}$$

where, f_R is equal to 0.115 for As_2S_3 chalcogenide glass, and $\tau_1 = 23.1$ fs and $\tau_2 = 1.95$ fs are two adjustable parameters.

The higher-order dispersion shows its important influence as the input pulse's center wavelength approaches ZDW and is computed through the development coefficients of the Taylor series around the center wavelength ω_0, the expansion of the propagation constant (β) can be obtained by [56]:

$$\beta_n = \left.\frac{d^n\beta}{d\omega^n}\right|_{\omega=\omega_0}. \tag{9}$$

Where $n = 2, 3, 4\ldots$ is the dispersion coefficient. Table 2 shows the higher-order dispersion at the pump pulse frequency in numerical modeling.

In this section, we study in detail how dispersion and nonlinear properties can affect the generation of quality SC spectra for the proposed fibers #F_1 and #F_2. For #F_1 fiber, the SC generation in the all-normal dispersion regime is pumped at 5.0 μm, the pulse duration is 90 fs, and the peak power varies from 1 kW to 6 kW (corresponding to input pulse energy from 0.09 nJ to 0.54 nJ). The pulse propagation length for the #F_1 fiber is 10 cm. Meanwhile, #F_2 fiber has anomalous dispersion regimes and the SC generation was analyzed with peak power ranging from 0.05 kW to 2 kW (corresponding to pulse energies from 0.01 nJ to 0.4 nJ, respectively) at a propagation length of 10 cm, and a pulse duration of 200 fs.

The spectral broadening in #F_1 fiber is induced by self-phase modulation (SPM) followed by optical wave breaking (OWB) as a typical mechanism for all-normal dispersion spectral broadening. Fig. 6 depicts the spectral broadening according to various peak power in the 10 cm #F_1 fiber sample. In the case of low input pulse energy, the SC spectrum is induced by SPM which is accompanied by an oscillatory structure covering the entire spectrum. The SPM-induced spectrum consists of many peaks and the outermost peak

Table 2
The coefficients of high-order chromatic dispersion at the pump wavelength.

Coefficient	#F_1	#F_2
β_2 (ps^2/m)	5.2×10^{-2}	-1.18×10^{-1}
β_3 (ps^3/m)	-4.79×10^{-4}	9.28×10^{-4}
β_4 (ps^4/m)	1.33×10^{-5}	1.77×10^{-6}
β_5 (ps^5/m)	-7.69×10^{-8}	-9.87×10^{-8}
β_6 (ps^6/m)	-1.55×10^{-9}	9.57×10^{-10}
β_7 (ps^7/m)	-6×10^{-11}	2.25×10^{-11}
β_8 (ps^8/m)	5.34×10^{-12}	-5.64×10^{-14}
β_9 (ps^9/m)	-5.08×10^{-14}	-3.78×10^{-14}
β_{10} (ps^{10}/m)	-5.71×10^{-15}	1.01×10^{-15}
β_{11} (ps^{11}/m)	2.36×10^{-16}	7.14×10^{-18}

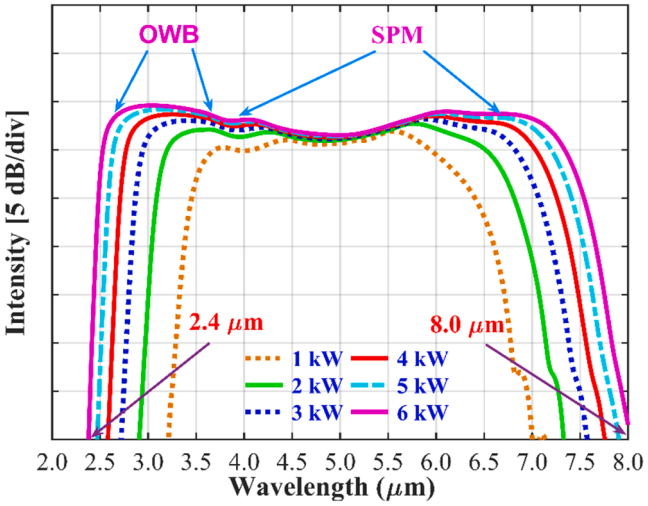

Fig. 6. The output spectra of fiber #F_1 for various peak power using pump pulses with 5.0 μm wavelength and 90 fs duration.

has the most intense, Fig. 6. With the further increase of the input peak power (higher than 1 kW), the center of the spectrum is induced by SPM, and then OBW contributes to the spectral broadening at the wings, Fig. 6. In the case of peak power of 6 kW, the SC spectrum spans in the wavelength range of 2.4–8.0 μm within 10 dB dynamics.

The fiber #F_2 has two zero-dispersion wavelengths with ZDW_1 at 5.5 μm and ZDW_2 at 16.2 μm. The SC generation was analyzed with a pump wavelength of 9.5 μm and a pulse width of 200 fs with a fiber propagation length of 10 cm. The #F_2 fiber has a pump wavelength in an anomalous dispersion regime so soliton dynamics, e.g. SF, SSFS will play an important role in the spectrum expansion. The solitons will shift further towards longer wavelengths if the process propagates further, which results in a very large extension of the received spectrum towards the red light region. Furthermore, through four-wave mixing the DW components are generated and lead to propagation without any frequency shift. The spectrum expansion with different peak powers is shown in Fig. 7. With peak power equal to 0.05 kW (input pulse energy 0.01 nJ), SPM plays a major role in spectrum expansion, so the resulting spectrum is small in this case. For peak power greater than 0.05 kW, soliton fission begins to appear and broadens the spectrum. As the peak power increases, the spectrum width increases. However, when the peak power is 2 kW (input pulse energy 0.4 nJ), the spectrum width is almost unchanged compared to the case where the peak power is 1.5 kW. This is explained by factors such as a high dispersion gradient in the short-wavelength range, low nonlinear coefficient, and high loss in the long-wavelength range. When the peak power is equal to 2 kW, the SCG has multi octave-spanning, from 4.4 μm to 16 μm within 10 dB dynamics, Fig. 7.

A comparison of the SC range in this work and previous studies is shown in Table 3. The proposed fibers offer the multi-octave spanning SCG with much lower input peak power when compared to previous works [51–55]. In the all-normal dispersion regime, #F_1 fiber can achieve a larger bandwidth than the compared works but uses approximately the same peak power [52–54]. In particular, the fiber in Ref. [51] has a spectrum broadening from 1.05 μm to 5.05 μm with a peak power of 28.16 kW, while the proposed fiber #F_1 has a spectrum broadening from 2.4 μm to 8.0 μm but uses a lower peak power of 4.7 times compared to the Ref. [51]. PCF with all-normal dispersion regime in Ref. [55] used a peak power of 10 kW and was 1.7 times larger than our work, but the obtained spectral range was 5 times smaller than that of fiber #F_1. For the anomalous dispersion regime, the SC spectrum obtained in the #F_2 fiber has a peak power 100 times lower and 3.6 times broader than in Ref. [55].

The low input peak power and large core give the proposed fibers a high potential for a compact all-fiber SCG system. The SCG in proposed fibers has a potential for high coherence. Thus, they are possible to use for applications in the mid-IR range, such as multimodal biophotonic imaging, and multibeam pump-probe techniques.

5. Conclusions

In this paper, we designed a novel photonic crystal fiber (PCF) using Chalcogenide glass. The characteristic properties of the square lattice PCF are controlled by varying the filling factor (d/Λ) and lattice constant (Λ). The proposed PCFs were selected from the preliminary fiber design with modification of the structural parameters. The two proposed fibers have flat dispersion, close to zero dispersion, low loss, and high nonlinear coefficient facilitating high-performance SCG generation with low input peak power.

The fiber #F_1 operates in an all-normal dispersion regime, characterized by a lattice constant of 1.0 μm and a filling factor of 0.3. #F_1 has flat dispersion, a small dispersion value of −92.3 ps/nm/km, high nonlinear coefficient of 120.44 $W^{-1}.km^{-1}$ obtained at pump wavelength 5.0 μm. The dominant effect driving the SC spectrum expansion for #F_1 fiber is SPM followed by OWB. The obtained SC spectrum extends from 2.4 μm to 8.0 μm with a low peak power of 6 kW of an ultrashort pulse propagating in a 10 cm long pass fiber.

Meanwhile, the #F_2 fiber exhibits anomalous dispersion regimes. Soliton dynamics including SF, SSFS, and DW are the main effects that make the SC spectrum of #F_2 much wider than that of #F_1 fiber. With a low peak power of 2 kW and a pulse duration of 200 fs, the

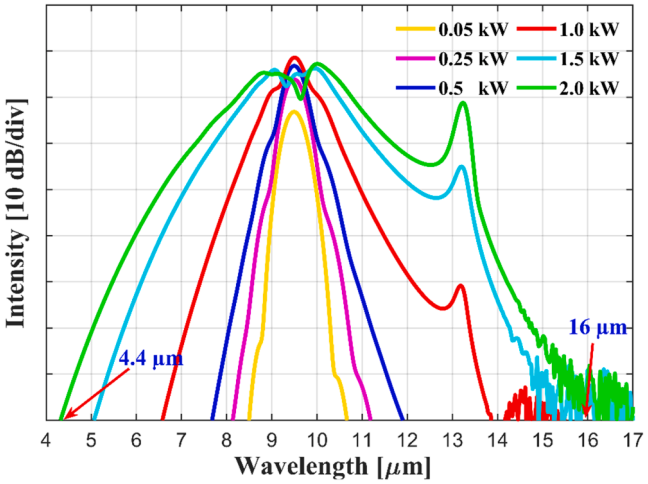

Fig. 7. The output spectra of fiber #F_2 for various peak power when using pump pulses with 9.5 μm wavelength and 200 fs duration.

Table 3
Comparison of the SC generated in the proposed As_2S_3 against other recent ChG PCF designs.

ChG glass	*Peak power (kW)*	*Pump wavelength* (μm)	*SC spectral range (μm)*	*Regime*
#F_1 [this work]	6	5.0	2.4 – 8.0	All-normal
#F_2 [this work]	2	9.5	4.4– 16	Anomalous
As_2S_5 [51]	28.16	2.5	1.05 – 5.05	All-normal
As_2Se_3 [52]	4.25	4.37	3.86 – 5.95	All-normal
$As_{39}Se_{61}$ [53]	5	3.45	1.95 – 6.58	All-normal
As_2S_3 [54]	5	2	0.96 – 2.91	All-normal
$Ge_{11.5}As_{24}Se_{64.5}$/ $Ge_{20}Sb_{15}Se_{65}$ [55]	10	1.3	0.8–1.9	All-normal
$Ge_{11.5}As_{24}Se_{64.5}$/ $Ge_{20}Sb_{15}Se_{65}$ [55]	200	3	1.6–4.8	Anomalous

obtained #F_2 SC spectrum is in the range from 4.4 μm to 16 μm within 10 dB propagating in a 10 cm long fiber.

The combination of low input peak power and large core in our proposed fibers presents a significant potential for a compact all-fiber SCG system. Additionally, the SCG achieved in these fibers demonstrates high coherence, further enhancing their suitability for various applications in the mid-IR range. These applications include but are not limited to multimodal biophotonic imaging and multibeam pump-probe techniques.

Declaration of Competing Interest

The authors declare that they have no known competing financial interests or personal relationships that could have appeared to influence the work reported in this paper.

Acknowledgments

This research is supported by Vietnam National Foundation for Science and Technology Development (NAFOSTED) under grant number 103.03-2023.01.

Data availability

No data was used for the research described in the article.

References

[1] G.P. Agrawal, Nonlinear fiber optics, Fifth edition, Elsevier, Amsterdam, 2013, 10.1016/C2011-0-00045-5.
[2] K.E. Jahromi, Q. Pan, L. Høgstedt, S.M. Friis, A. Khodabakhsh, P.M. Moselund, F.J. Harren, Mid-infrared supercontinuum-based upconversion detection for trace gas sensing, Opt. Express 27 (17) (2019) 24469–24480, https://doi.org/10.1364/OE.27.024469.
[3] J. Yuan, Z. Kang, F. Li, X. Zhang, X. Sang, Q. Wu, B. Yan, K. Wang, X. Zhou, K. Zhong, G. Zhou, C. Yu, C. Lu, H.Y. Tam, P.K.A. Wai, Mid-infrared octave-spanning supercontinuum and frequency comb generation in a suspended germanium-membrane ridge waveguide, J. Light. Technol. 35 (14) (2017) 2994–3002, https://doi.org/10.1364/CLEO_AT.2016.JTh2A.89.

[4] R.R. Alfano, S.L. Shapiro, Observation of self-phase modulation and small-scale filaments in crystals and glasses, Phys. Rev. Lett. 24 (11) (1970) 592–594. ⟨https://link.aps.org/doi/10.1103/PhysRevLett.24.592⟩.

[5] C. Nicolas, D. Alexandre, C. Guillaume, D. Mathieu, R. William, A.G. Claire, L. Sidonie, F. Julien, Supercontinuum laser absorption spectroscopy in the mid-infrared range for identification and concentration estimation of a multi-component atmospheric gas mixture, Proc. SPIE 8182 (2011), https://doi.org/10.1117/12.898227.

[6] C. Amiot, A. Aalto, P. Ryczkowski, J. Toivonen, G. Genty, Cavity enhanced absorption spectroscopy in the mid-infrared using a supercontinuum source, Appl. Phys. Lett. 111 (6) (2017) 061103, https://doi.org/10.1063/1.4985263.

[7] E.K. Jahromi, M. Nematollahi, Q. Pan, M.A. Abbas, S.M. Cristescu, F.J.M. Harren, A. Khodabakhsh, Sensitive multi-species trace gas sensor based on a high repetition rate mid-infrared supercontinuum source, Opt. Express 28 (18) (2020) 26091–26101, https://doi.org/10.1364/OE.396884.

[8] A.B. Seddon, A prospective for new mid-infrared medical endoscopy using chalcogenide glasses, Int. J. Appl. Glas Sci. 2 (3) (2011) 177–191, https://doi.org/10.1111/j.2041-1294.2011.00059.x.

[9] P. Moselund, C. Petersen, S. Dupont, C. Agger, O. Bang, S.R. Keiding, Supercontinuum: broad as a lamp, bright as a laser, now in the mid-infrared, Proc. SPIE (2012) 83811A, https://doi.org/10.1117/12.920094.

[10] C.R. Petersen, N. Prtljaga, M. Farries, J. Ward, B. Napier, G.R. Lloyd, J. Nallala, N. Stone, O. Bang, Mid-infrared multispectral tissue imaging using a chalcogenide fiber supercontinuum source, Opt. Lett. 43 (5) (2018) 999–1002, https://doi.org/10.1364/OL.43.000999.

[11] C.S. Cheung, J.M.O. Daniel, M. Tokurakawa, W.A. Clarkson, H. Liang, High resolution Fourier domain optical coherence tomography in the 2 μm wavelength range using a broadband supercontinuum source, Opt. Express 23 (3) (2015) 1992–2001, https://doi.org/10.1364/OE.23.001992.

[12] N.M. Israelsen, C.R. Petersen, A. Barh, D. Jain, M. Jensen, G. Hannesschläger, P.T. Lichtenberg, C. Pedersen, A. Podoleanu, O. Bang, Real-time high-resolution mid-infrared optical coherence tomography, Light Sci. Appl. 8 (11) (2019) 11–24, https://doi.org/10.1038/s41377-019-0122-5.

[13] A. Schliesser, N. Picqué, T.W. Hänsch, Mid-infrared frequency combs, Nat. Photonics 6 (7) (2012) 440–449, https://doi.org/10.1038/nphoton.2012.142.

[14] K. Park, J. Na, J. Kim, Y. Jeong, Numerical study on supercontinuum generation in an active highly nonlinear photonic crystal fiber with anomalous dispersion, IEEE J. Quantum Electron. 56 (2) (2020) 6800109–6800118, https://doi.org/10.1109/JQE.2020.2974519.

[15] C.V. Lanh, L.V. Hieu, D.V. Nguyen, V.T.M. Ngoc, H.D. Quang, H.V. Thuy, N.V. Thuy, C.V. Bien, Modelling of lead-bismuth gallate glass ultra-flatted normal dispersion photonic crystal fiber infiltrated with tetrachloroethylene for high coherence mid-infrared supercontinuum generation, Laser Phys. 32 (2022) 055102–055114, https://doi.org/10.1088/1555-6611/ac599b.

[16] M. Vieweg, T. Gissibl, S. Pricking, B.T. Kuhlmey, D.C. Wu, B.J. Eggleton, H. Giessen, Ultrafast nonlinear optofluidics in selectively liquid-filled photonic crystal fibers, Opt. Express 18 (24) (2010) 25232–25240, https://doi.org/10.1364/OE.18.025232.

[17] Y. Huang, Y. Xu, A. Yariv, Fabrication of functional microstructured optical fibers through a selectivefilling technique, Appl. Phys. Lett. 85 (22) (2004) 5182–5184, https://doi.org/10.1063/1.1828593.

[18] F. Wang, W. Yuan, O. Hansen, O. Bang, Selective filling of photonic crystal fibers using focused ion beam milled microchannels, Opt. Express 19 (18) (2011) 17585–17590, https://doi.org/10.1364/OE.19.017585.

[19] L. Xiao, W. Jin, M. Demokan, H. Ho, Y. Hoo, C. Zhao, Fabrication of selective injection microstructured optical fibers with a conventional fusion splicer, Opt. Express 13 (22) (2005) 9014–9022, https://doi.org/10.1364/OPEX.13.009014.

[20] L.V. Hieu, H.V. Thuy, N.T. Hue, C.L. Van, R. Buczyński, R. Kasztelanic, Supercontinuum generation in photonic crystal fibers infltrated with tetrachloroethylene, Opt. Quantum Electron 53 (2021) 187–205, https://doi.org/10.1007/s11082-021-02820-3.

[21] L.V. Hieu, H.V. Thuy, L.C. Trung, H.D. Quang, N.T. Hue, V.T.M. Ngoc, M. Klimczak, R. Buczyński, R. Kasztelanic, Silica-based photonic crystal fiber infiltrated with 1,2-dibromoethane for supercontinuum generation, Appl. Opt. 60 (24) (2021) 7268–7278, https://doi.org/10.1364/AO.430843.

[22] L.T.B. Tran, T.T.C. Oanh, N.T. Thuy, C.V. Lanh, Comparison of chromatic dispersion of circular and hexagonal photonic crystal fibers with chloroform-core, Majlesi J. Electr. Eng. 16 (3) (2022) 55–61, https://doi.org/10.30486/mjee.2022.696507.

[23] C.V. Lanh, N.T. Thuy, H.T. Duc, L.T.B. Tran, V.T.M. Ngoc, D.V. Trong, L.C. Trung, H.D. Quang, D.Q. Khoa, Comparison of supercontinuum spectrum generating by hollow core PCFs filled with nitrobenzene with different lattice types, Opt. Quantum Electron. 54 (2022) 300–317, https://doi.org/10.1007/s11082-022-03667-y.

[24] C.V. Lanh, L.T.B. Tran, D.V. Trong, V.T.M. Ngoc, N.T. Thuy, N.T.H. Phuong, T.N.M. Hang, H.V. Thuy, Supercontinuum generation in highly birefringent fiber infiltrated with carbon disulfide, Opt. Fiber Technol. 75 (2023) 103151–103161, https://doi.org/10.1016/j.yofte.2022.103151.

[25] L.V. Hieu, H.V. Thuy, G. Stępniewski, L.C. Trung, V.T.M. Ngoc, R. Kasztelanic, M. Klimczak, J. Pniewski, D.X. Khoa, A.M. Heidt, R. Buczyński, Low pump power coherent supercontinuum generation in heavy metal oxide solid-core photonic crystal fibers infiltrated with carbon tetrachloride covering 930–2500nm, Opt. Express 29 (24) (2021) 39586–39600, https://doi.org/10.1364/OE.443666.

[26] T.L. Myers, R.G. Tonkyn, T.O. Danby, M.S. Taubman, B.E. Bernacki, J.C. Birnbaum, S.W. Sharpe, T.J. Johnson, Accurate measurement of the optical constants n and k for a series of 57 inorganic and organic liquids for optical modeling and detection, Appl. Spectrosc. 72 (4) (2018) 535–550, https://doi.org/10.1177/0003702817742848.

[27] N.T. Thuy, H.T. Duc, L.T.B. Tran, D.V. Trong, C.V. Lanh, Optimization of optical properties of toluene-core photonic crystal fibers with circle lattice for supercontinuum generation, J. Opt. 51 (2022) 678–688, https://doi.org/10.1007/s12596-021-00802-y.

[28] P.S. Maji, P.R. Chaudhuri, Studies of the modal properties of circularly photonic crystal fiber (C-PCF) for high power applications, Photon Nanostruct. Fundam. Appl. 19 (2016) 12–23, https://doi.org/10.1016/j.photonics.2016.01.004.

[29] A. Rjeb, H. Fathallah, S. Chebaane, M. Machhout, Design of novel circular lattice photonic crystal fiber suitable for transporting 48 OAM modes, Optoelectron. Lett. 17 (8) (2021) 501–506, https://doi.org/10.1007/s11801-021-0158-7.

[30] S.K. Pandey, S. Singh, Y.K. Prajapati, A novel PCF design with an ultra-fattened dispersion and low confnement loss by varying tiny air-hole concentration at core and cladding, Opt. Rev. 28 (2021) 304–313, https://doi.org/10.1007/s10043-021-00662-8.

[31] H. Saghaei, A. Ghanbari, White light generation using photonic crystal fiber with sub-micron circular lattice, J. Electr. Eng. 68 (4) (2017) 282–289, https://doi.org/10.1515/jee-2017-0040.

[32] A. Medjouri, L.M. Simohamed, O. Ziane, A. Boudrioua, Z. Becer, Design of a circular photonic crystal fiber with flattened chromatic dispersion using a defected core and selectively reduced air holes: application to supercontinuum generation at 1.55 μm, Photon. Nanostruct. Fundam. Appl. 16 (2015) 43–50, https://doi.org/10.1016/j.photonics.2015.08.004.

[33] K. Saitoh, M. Koshiba, T. Hasegawa, E. Sasaoka, Chromatic dispersion control in photonic crystal fibers: application to ultra-flattened dispersion, Opt. Express 11 (8) (2003) 843–852, https://doi.org/10.1364/OE.11.000843.

[34] K. Moutzouris, M. Papamichael, S.C. Betsis, I. Stavrakas, G. Hloupis, D. Triantis, Refractive, dispersive and thermo-optic properties of twelve organic solvents in the visible and near-infrared, Appl. Phys. 116 (2014) 617–622, https://doi.org/10.1007/s00340-013-5744-3.

[35] S. Kedenburg, M. Vieweg, T. Gissibl, H. Giessen, Linear refractive index and absorption measurements of nonlinear optical liquids in the visible and near-infrared spectral region, Opt. Mater. Express 2 (11) (2012) 1588–1611, https://doi.org/10.1364/OME.2.001588.

[36] Y. Huang, H. Yanga, S. Zhao, Y. Mao, S. Chen, Design of photonic crystal fibers with flat dispersion and three zero dispersion wavelengths for coherent supercontinuum generation in both normal and anomalous regions, Results Phys. 23 (2021) 104033–104043, https://doi.org/10.1016/j.rinp.2021.104033.

[37] H.D. Quang, J. Pniewski, L.V. Hieu, A. Ramaniuk, L.C. Van, K. Borzycki, D.X. Khoa, M. Klimczak, R. Buczyński, Optimization of optical properties of photonic crystal fibers infiltrated with carbon tetrachloride for supercontinuum generation with subnanojoule femtosecond pulses, Appl. Opt. 57 (14) (2018) 3738–3746, https://doi.org/10.1364/AO.57.003738.

[38] C.V. Lanh, A. Anuszkiewicz, A. Ramaniuk, R. Kasztelanic, D.X. Khoa, M. Trippenbach, R. Buczyński, Supercontinuum generation in photonic crystal fibres with core filled with toluene, J. Opt. 19 (12) (2017), https://doi.org/10.1088/2040-8986/aa96bc.

[39] C.V. Lanh, H.V. Thuy, C.L. Van, K. Borzycki, D.X. Khoa, T.Q. Vu, M. Trippenbach, R. Buczyński, R. Pniewski, Optimization of optical properties of photonic crystal fibers infiltrated with chloroform for supercontinuum generation, Laser Phys. 29 (7) (2019) 075107–075116, https://doi.org/10.1088/1555-6611/ab2115.

[40] L. Tian, L. Wei, F. Guoying, Numerical simulation of supercontinuum generation in liquid-filled photonic crystal fibers with a normal flat dispersion profile, Opt. Commun. 334 (2015) 196–202, https://doi.org/10.1016/j.optcom.2014.07.080.
[41] C.V. Lanh, N.T. Thuy, L.T.B. Tran, H.T. Duc, V.T.M. Ngoc, L.V. Hieu, H.V. Thuy, Multi-octave supercontinuum generation in As_2Se_3 chalcogenide photonic crystal fiber, Photon. Nanostruct. - Fundam. Appl. 48 (2022) 100986, https://doi.org/10.1016/j.photonics.2021.100986.
[42] C.R. Petersen, U. Møller, I. Kubat, B. Zhou, S. Dupont, J. Ramsay, T. Benson, S. Sujecki, N.A. Moneim, Z. Tang, D. Furniss, Mid-infrared supercontinuum covering the 1.4-13.3 μm molecular fingerprint region using ultra-high NA chalcogenide step-index fibre, Nat. Photon. 8 (11) (2014) 830, https://doi.org/10.1038/nphoton.2014.213.
[43] M. Liao, C. Chaudhari, L. Shuo, L.S. Guang, Numerical analysis of photonic crystal fiber with chalcogenide core tellurite cladding composite microstructure, Chin. Phys. B. 22 (2013) 074206, https://doi.org/10.1088/1674-1056/22/7/074206.
[44] T.S. Saini, A. Baili, A. Kumar, R. Cherif, M. Zghal, R.K. Sinha, Design and analysis of equiangular spiral photonic crystal fiber for mid-infrared supercontinuum generation, J. Mod. Opt. 62 (2015) 1570–1576, https://doi.org/10.1080/09500340.2015.1051600.
[45] A.B. Salem, R. Cherif, M. Zghal, Tapered As_2S_3 chalcogenide photonic crystal fiber for broadband mid-infrared supercontinuum generation. Frontiers in Optics 2011/Laser Science XXVII, OSA Technical Digest (Optical Society of America, 2011, p. FMG6, https://doi.org/10.1364/FIO.2011.FMG6.
[46] T.S. Saini, A. Kumar, R.K. RSinha, Design and modeling of dispersion engineered rib waveguide for ultra-broadband mid-infrared supercontinuum generation, J. Mod. Opt. 64 (2) (2017) 143–149, https://doi.org/10.1080/09500340.2016.1216190.
[47] J.W. Choi, Z. Han, B.U. Sohn, G.F.R. Chen, C. Smith, L.C. Kimerling, K.A. Richardson, A.M. Agarwal, D.T.H. Tan, Nonlinear characterization of Ge-Sb-S chalcogenide glass waveguides, Sci. Rep. 6 (2016) 39234, https://doi.org/10.1038/srep39234.
[48] ⟨https://www.ansys.com/products/optics/mode⟩.
[49] S. Liu, L. Jin, W. Jin, D. Wang, C. Liao, Y. Wang, Structural long period gratings made by drilling micro-holes in photonic crystal fibers with a femtosecond infrared laser, Opt. Express 18 (6) (2010) 5496–5503, https://doi.org/10.1364/OE.18.005496.
[50] M.M. Hassan, K. Ahmed, B.K. Paul, M.N. Hossain, F.A.A. Zahrani, Anomalous birefringence and nonlinearity enhancement of As_2S_3 and As_2S_5 filled D-shape fiber for optical communication, Phys. Scr. 96 (2021) 115501, https://doi.org/10.1088/1402-4896/ac13e1.
[51] A.B. Salem, M. Diouf, R. Cherif, A. Wague, M. Zghal, Ultraflat-top midinfrared coherent broadband supercontinuum using all normal As_2S_5-borosilicate hybrid photonic crystal fiber, Opt. Eng. 55 (2016) 066109, https://doi.org/10.1117/1.OE.55.6.066109.
[52] E. Wang, J. Li, J. Li, Q. Cheng, X. Zhou, H. Jiang, Flattened and broadband mid-infrared supercontinuum generation in As_2Se_3 based holey fiber, Opt. Quantum Electron. 51 (2019) 1–13, https://doi.org/10.1007/s11082-018-1722-7.
[53] A. Medjouri, D. Abed, Design and modelling of all-normal dispersion $As_{39}Se_{61}$ chalcogenide photonic crystal fiber for flat-top coherent mid-infrared supercontinuum generation, Opt. Fiber Technol. 50 (2019) 154–164, https://doi.org/10.1016/j.yofte.2019.03.021.
[54] W. Geng, C. Bao, Y. Fang, Y. Wang, Y. Li, Z. Wang, Y.G. Liu, H. Huang, Y. Ren, Z. Pan, Y. Yue, 1.6-octave coherent OAM supercontinuum generation in As_2S_3 photonic crystal fiber, IEEE Access 8 (2020) 168177–168185, https://doi.org/10.1109/ACCESS.2020.3023133.
[55] A. Cheshmberah, M. Seifouri, S. Olyaee, Design of all-normal dispersion with $Ge_{11.5}As_{24}Se_{64.5}/Ge_{20}Sb_{15}Se_{65}$ chalcogenide PCF pumped at 1300 nm for supercontinuum generation, Otp. Quant. Electo 53 (2021) 461, https://doi.org/10.1007/s11082-021-03099-0.